Cement and Concrete Research 40 (2010) 1120–1128

Contents lists available at ScienceDirect

Cement and Concrete Research

journal homepage: http://ees.elsevier.com/CEMCON/default.asp

Characterization of pore structure in cement-based materials using pressurization–depressurization cycling mercury intrusion porosimetry (PDC-MIP)

Jian Zhou [a,*], Guang Ye [a,b,1], Klaas van Breugel [a,2]

[a] Microlab, Faculty of Civil Engineering and Geosciences, Delft University of Technology, Delft, The Netherlands
[b] Magnel Laboratory for Concrete Research, Department of Structural Engineering, Ghent University, Technologiepark-Zwijnaarde 904 B-9052, Ghent (Zwijnaarde), Belgium

ARTICLE INFO

Article history:
Received 2 July 2009
Accepted 19 February 2010

Keywords:
Pore size distribution (B)
Mercury porosimetry (B)
Cement paste (D)
Pressurization–depressurization cycling

ABSTRACT

Numerous mercury intrusion porosimetry (MIP) studies have been carried out to investigate the pore structure in cement-based materials. However, the standard MIP often results in an underestimation of large pores and an overestimation of small pores because of its intrinsic limitation. In this paper, an innovative MIP method is developed in order to provide a more accurate estimation of pore size distribution. The new MIP measurements are conducted following a unique mercury intrusion procedure, in which the applied pressure is increased from the minimum to the maximum by repeating pressurization–depressurization cycles instead of a continuous pressurization followed by a continuous depressurization. Accordingly, this method is called pressurization–depressurization cycling MIP (PDC-MIP). By following the PDC-MIP testing sequence, the volumes of the throat pores and the corresponding ink-bottle pores can be determined at every pore size. These values are used to calculate pore size distribution by using the newly developed analysis method. This paper presents an application of PDC-MIP on the investigation of the pore size distribution in cement-based materials. The experimental results of PDC-MIP are compared with those measured by standard MIP. The PDC-MIP is further validated with the other experimental methods and numerical tool, including nitrogen sorption, backscanning electron (BSE) image analysis, Wood's metal intrusion porosimetry (WMIP) and the numerical simulation by the cement hydration model HYMOSTRUC3D.

1. Introduction

Cementitious materials react with water, producing hydration products at the surface of cement particles and growing into the initially-water-filled space. The main hydration product (C–S–H) is a colloidal amorphous gel and contains pores, which are called gel pores [1]. The gel pore has a size of approximately several nanometers. The empty or initially-water-filled space is called capillary pore. The capillary pore has a size ranging from several nanometers to several micrometers. Many properties of cement-based materials are directly or indirectly related to pore structure [2]. Generally speaking, strength and elasticity are principally a function of the total porosity. The total porosity, shape, size and connectivity of pores determine water and ionic transport and they thus govern the permeability, diffusivity and durability of cement-based materials. The pore structure also has influence on shrinkage and creep. Therefore, correct characterization of the pore structure is of great importance to interpret the properties of cement-based materials.

Mercury intrusion porosimetry (MIP) has become one of the most widely used methods for investigating the pore structure in cement-based materials since the work of Winslow and Diamond in the 1970s [3]. The standard MIP measurement is conducted as follows. Samples are first dried in order to remove water from pores. The dried samples are weighted and placed into a chamber. The chamber is evacuated to remove air from the samples. Then mercury fills up the chamber. As the applied pressure is increased, mercury is forced to intrude into the samples gradually. The mercury intrusion volumes and the corresponding applied pressures are recorded at every pressure steps. The mercury intrusion volume and the corresponding applied pressure provide the basic data for the analysis of pore structure. With the assumption that pores are cylindrical and entirely and equally accessible to mercury, the applied pressure can be converted into the pore diameter by using the Washburn equation [4],

$$D = \frac{-4\gamma\cos\theta}{P} \tag{1}$$

where, D is the equivalent pore diameter, P is the applied pressure, γ is the surface tension of mercury and θ is the contact angle between mercury and solids.

* Corresponding author. Tel.: +31 15 2784001; fax: +31 15 2786383.
E-mail addresses: Jian.Zhou@tudelft.nl (J. Zhou), g.ye@tudelft.nl (G. Ye), k.vanbreugel@tudelft.nl (K. van Breugel).
[1] Tel.: +31 15 2784001; fax: +31 15 2786383.
[2] Tel.: +31 15 2784954; fax: +31 15 2786383.

0008-8846/$ – see front matter © 2010 Elsevier Ltd. All rights reserved.
doi:10.1016/j.cemconres.2010.02.011

Fig. 1 gives an example of the experimental results of a standard MIP measurement on a Portland cement paste with a water-to-cement (w/c) ratio of 0.4 at 28 days. The solid line is the cumulative mercury intrusion curve, also called cumulative porosity curve. In this curve, the volumes of mercury intrusion are plotted against the pore diameters. The total porosity can be calculated by dividing the total intruded volume by the bulk volume of the sample. By differentiating the cumulative pore volume by the logarithmic pore diameter, the pore size distribution curve (dash line in Fig. 1) can be obtained. Several peaks, usually two principal peaks, are often observed in the pore size distribution curve, which correspond to the steepest slopes in the cumulative pore volume curve. The pore diameters corresponding to these peaks are called critical pore size [5], which is an important parameter used to describe transport properties.

Aforementioned, MIP is based on the Washburn equation and the assumption that pores are cylindrical and entirely and equally accessible to mercury. Therefore, the MIP measurement can only provide a valid estimation of pore structure, when the sample has the property that each pore is directly accessible to mercury or can be reached by mercury through larger pores [6,7]. However, microscopy study revealed that the pore size of cement-based materials is randomly distributed and most pores are connected to the surface of the sample through a chain of pores with varying sizes and shapes [6]. With such a pore structure, mercury can not intrude into larger pores until the applied pressure is sufficient to force mercury to go through smaller throats. As a result, the volume of these larger pores is counted as the volume of smaller throats. This is referred to as the "accessibility effect" [6]. The larger pores that are accessible to mercury through smaller throats are called ink-bottle pores. And, the smaller throats are called throat pores. The ink-bottle pores and the throat pores constitute the total porosity. The minimum size of pores detected by MIP is about 7 nm. Mindess and Young suggested that pores smaller than 10 nm do not contribute to water and ionic transport [1]. Therefore, the pores smaller than 7 nm are not considered in this paper.

The "accessibility effect" can be illustrated with two imaginary pore systems as shown in Fig. 2. Each of them consists of a large pore (with a diameter of d_1 and a volume of v_1) and a small pore (with a diameter of d_2 and a volume of v_2). In Fig. 2 (left), the large pore is directly connected to mercury. During an MIP measurement, the large pore is filled with mercury when the applied pressure is increased to p_1. The small pore is filled with mercury when the applied pressure is increased to p_2. For this pore system, the MIP result can reveal the real pore size distribution. In contrast, in Fig. 2 (right), the large pore is connected to mercury through the small pore. An applied pressure of

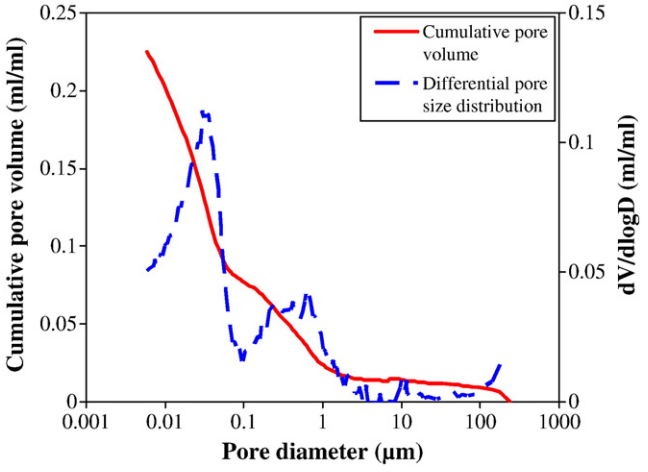

Fig. 1. Experimental results of a standard MIP measurement of a 28-day-old 0.4-w/c-ratio Portland cement paste.

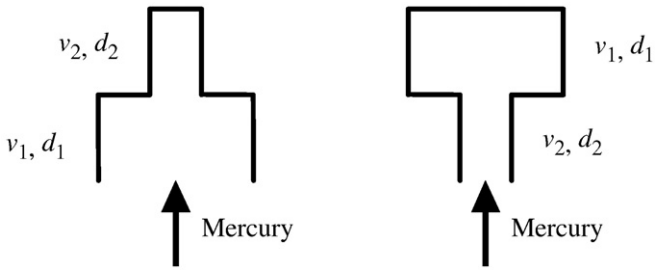

Fig. 2. Schematic illustration of two imaginary pore systems with a large pore and a small pore.

p_1 is not big enough to force mercury to intrude into the large pore. Only when the applied pressure is increased to p_2, mercury intrudes into both the large and small pores. Consequently, this MIP measurement result shows that the volume of the large pore is zero, and the volume of the small pore equals to $v_1 + v_2$. As a result, the MIP measurement provides an underestimation of the volume of the large pore and an overestimation of the volume of the small pore.

This paper aims to develop a new MIP method, which can overcome the "accessibility effect" and provide a more accurate estimation of the pore size distribution in cement-based materials. This method consists of a unique testing sequence and a new data analysis method. The unique MIP testing sequence is conducted by repeating pressurization–depressurization cycles. The applied pressure is increased from the minimum to the maximum cycle by cycle. Accordingly, this method is called pressurization–depressurization cycling MIP (PDC-MIP). In the following sections, the previous works on improving MIP are overviewed. Then, PDC-MIP is introduced. Section 4 describes the experiments used to validate PDC-MIP. In Section 5, the experimental results measured with the PDC-MIP testing sequence are reported and compared with those of the standard MIP testing sequence. Moreover, the experimental results are used to calculate pore size distribution using the PDC-MIP data analysis method. PDC-MIP is further validated in Section 6 with other experimental techniques and numerical tool, including nitrogen sorption, backscanning electron (BSE) image analysis, Wood's metal intrusion porosimetry (WMIP) and numerical simulation by the cement hydration model HYMOSTRUC3D. Although the PDC-MIP is demonstrated with an application in cement-based materials, its application is not limited to cement-based materials and may be used in other porous materials.

2. Previous studies on improving MIP method

Many researchers have spent effort on improving MIP to eliminate the impact of the "accessibility effect". Liu and Winslow [8] intruded mercury progressively to the maximum pressure, then reduced the pressure progressively to the minimum pressure, and re-intruded to the maximum pressure. They found that the processes of mercury extrusion and re-intrusion were fully reversible when appropriate advancing and receding contact angles were used. They suggested that the pore system of cement paste can be divided into two parts, i.e. reversibly and irreversibly intruded pores. The reversibly intruded pores were more accessible to mercury and more closely correlated with the transport properties of cement-based materials. Yoshida and Kishi [9] have recently developed a method to determine the volumes of connective pores and disconnective pores. The measurement began progressively with a pressurization to a certain pressure. The applied pressure was then decreased until the minimum pressure is reached. The applied pressure was increased again to a pressure higher than that of the previous pressurization, and the applied pressure was decreased again to the minimum pressure. This cycle was repeated 10 times until the maximum pressure of 412 MPa. By using this testing sequence, they divided the pore structure into connective capillary

pores and disconnective pores. Although the above two studies made a big progress in the characterization of pore structure in cement-based materials using MIP, these methods could not provide a valid estimation of pore size distribution.

3. PDC-MIP

The PDC-MIP method consists of the PDC-MIP testing sequence and the PDC-MIP data analysis method. PDC-MIP is introduced in this section by describing these two aspects in details.

3.1. PDC-MIP testing sequence

As illustrated in Fig. 3, the PDC-MIP measurement is conducted following a unique mercury intrusion procedure, in which the applied pressure is increased from the minimum to the maximum by repeating pressurization–depressurization cycles. In the nth pressurization–depressurization cycle, pressure is first increased to P_n^{in} and then decreased to P_n^{ex}. In the next cycle, pressure is increased to P_{n+1}^{in}. The pressurization–depressurization cycle is repeated until the maximum pressure. Within each pressurization–depressurization cycle, the mercury intrusion and extrusion volumes are recorded as V_n^{in} and V_n^{ex}, respectively. Here, the intrusion pressure P_n^{in} and extrusion pressure P_n^{ex} corresponding to the same pore diameter of D_n are calculated by using the Washburn equation with the different advancing and receding contact angles. When mercury advances across and recedes from the same surface, it has different contact angles. This leads to a hysteresis between the mercury intrusion and extrusion processes. The advancing and receding contact angles used in this paper were calculated with the pressures at which mercury intrudes into and extrudes out of an artificial straight cylindrical pore with known diameter [10].

Following this testing sequence, when the applied pressure is increased to P_n^{in}, mercury intrudes into both the throat pores with a diameter of D_n and the ink-bottle pores behind these throat pores. Then, the applied pressure is decreased to P_n^{ex}, and only the mercury in the throat pores with a diameter of D_n comes out. The rest newly intruded mercury remains in the ink-bottle pores. Consequently, V_n^{ex} equals to the volume of the throat pores with a diameter of D_n. And, $V_n^{in} - V_n^{ex}$ equals to the volume of the corresponding ink-bottle pores. This can be expressed as follows:

$$V_n^{th} = V_n^{ex} \tag{2}$$

$$V_n^{ink} = V_n^{in} - V_n^{ex} \tag{3}$$

where, V_n^{th} is the volume of the throat pores with a diameter of D_n, and V_n^{th} is the volume of the corresponding ink-bottle pores.

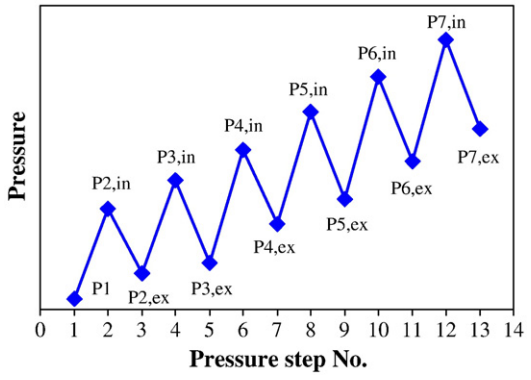

Fig. 3. Illustration of the PDC-MIP testing sequence with pressurization–depressurization cycles.

3.2. PDC-MIP data analysis method

By repeating the pressurization–depressurization cycles described in Section 3.1, the volumes of throat pores and ink-bottle pores can be measured at each throat pore diameter. Although the pore size distribution of the ink-bottle pores is not able to be determined, it is known that the ink-bottle pores have a diameter larger than the corresponding throat pores. In order to calculate the pore size distribution, an assumption is introduced: the size distribution of the ink-bottle pores is equal to that of the pores with the diameter larger than the corresponding throat pores, i.e. from D_1 to D_{n-1}. The pore size distribution can be recalculated as follows:

Step 1 Let $V_{1,1}$ be equal to V_1^{th}. The largest pores do not have the ink-bottle pores.

$$V_{1,1} = V_1^{th} - V_1^{ex} \tag{4}$$

where, $V_{1,1}$ is the volume of the pore with the diameter of D_1 calculated at Step 1.

Step 2 Let $V_{2,2}$ be equal to V_2^{th} and distribute the ink-bottle pore volume V_2^{ink} into the pores larger than D_2.

$$V_{2,2} = V_2^{th} = V_2^{ex} \tag{5a}$$

$$V_{1,2} = V_{1.1} + V_2^{ink} = V_{1,1} + \left(V_2^{in} - V_2^{ex}\right) \tag{5b}$$

where, $V_{1,2}$ and $V_{2,2}$ are the volume of the pores with the diameter of D_1 and D_2 calculated at Step 2.

Step 3 Similar as Step 2.

$$V_{3,3} = V_3^{th} = V_3^{ex} \tag{6a}$$

$$V_{1,3} = V_{1,2}\left(1 + \frac{V_3^{ink}}{V_{1,2} + V_{2,2}}\right) = V_{1,2}\left(1 + \frac{V_3^{in} - V_3^{ex}}{V_{1,2} + V_{2,2}}\right) \tag{6b}$$

$$V_{2,3} = V_{2,2}\left(1 + \frac{V_3^{ink}}{V_{1,2} + V_{2,2}}\right) = V_{2,2}\left(1 + \frac{V_3^{in} - V_3^{ex}}{V_{1,2} + V_{2,2}}\right) \tag{6c}$$

where, $V_{1,3}$, $V_{2,3}$ and $V_{3,3}$ are the volumes of the pores with the diameter of D_1, D_2 and D_3 calculated at Step 3.

Step j Similar as Step 3.

$$V_{j,j} = V_j^{th} = V_j^{ex} \tag{7a}$$

$$V_{i,j} = V_{i,j-1}\left(1 + \frac{V_j^{ink}}{V_{1,j-1} + V_{2,j-1} + \cdots + V_{j-1,j-1}}\right) \tag{7b}$$

$$= V_{i,j-1}\left(1 + \frac{V_j^{in} - V_j^{ex}}{V_{1,j-1} + V_{2,j-1} + \cdots + V_{j-1,j-1}}\right)(i<j)$$

where, $V_{i,j}$ is the volume of the pores with the diameter of D_i calculated at Step j.

The recalculated pore volume is equal to the pore volume calculated at the last step:

$$V_m = V_{m,m} = V_m^{th} = V_m^{ex} \tag{8a}$$

$$V_i = V_{i,m} = V_{i,m-1}\left(1 + \frac{V_m^{\text{ink}}}{V_{1,m-1} + V_{2,m-1} + \cdots + V_{m-1,m-1}}\right) \quad (8b)$$
$$= V_{i,m-1}\left(1 + \frac{V_m^{\text{in}} - V_m^{\text{ex}}}{V_{1,m-1} + V_{2,m-1} + \cdots + V_{m-1,m-1}}\right)$$

where, m is the total number of pressure cycles.

As an example, PDC-MIP is used to check the imaginary pore system as shown in Fig. 2 (right). When the applied pressure is increased to P_2^{in}, mercury intrudes into the large pore and the small pore, and the intrusion volume V_2^{in} is recorded as $v_1 + v_2$. Then, when pressure is decreased to P_1^{ex}, only mercury in the small pore comes out, and the extrusion volume V_2^{ex} is recorded as v_2. With Eqs. (4)–(8a,8b), the pore volumes can be calculated: $V_1 = V_2^{\text{in}} - V_1^{\text{ex}} = v_1$ and $V_2 = V_2^{\text{ex}} = v_2$. Obviously, the results of PDC-MIP can provide an accurate estimation of the real pore size distribution of this imaginary pore system.

4. Experiments

4.1. Materials

Portland cement paste with the water-to-cement ratio of 0.4 was studied. The binder was a Portland cement CEM I 42.5 N according to European standard EN 197-1. CEM I 42.5 N and water were mixed with a HOBART® mixer at low speed for 1 min and at high speed for 2 min. Then the fresh paste was poured into plastic bottles, sealed with lids and placed in a climate box with a temperature of 20 °C. After 1, 3, 7 or 28 days of curing, the sample was split into small pieces of around 1 g. The samples for PDC-MIP, standard MIP and BSE measurements were freeze-dried. The samples were quickly frozen by immersing in liquid nitrogen for 5 min. Then, they were moved into a freeze-dryer with temperature of −24 °C and vacuum of 0.1 Pa. The sample was considered to be dry, until the water loss was below 0.01%/day. This period lasted for 10–20 days depending on w/c-ratio and curing age of the samples. Ye [11] suggested that the freeze-drying method causes less damage to the pore structure of Portland cement paste compared with the other common drying methods, i.e. oven drying and vacuum drying.

4.2. MIP measurement

PDC-MIP testing sequence began with a continuous pressurization from 0.004 MPa to 0.15 MPa. Then, one hundred pressurization–depressurization cycles were repeated, and pressure was increased from 0.15 MPa to 200 MPa. The pressure ranging from 0.004 MPa to 200 MPa was in logarithmic distribution. In every pressurization–depressurization cycle, the intrusion and extrusion pressure values were calculated using the Washburn equation with the different advancing and receding contact angles. In an experimental study [10], it was found that the advancing contact angle and receding contact angle between cement-based materials and mercury increase from 125.4° to 138.0° and from 118.8° to 128.0°, respectively, as the curing age increases from 1 to 28 days. The values given in Table 1 were used in the calculation of intrusion and extrusion pressures. The surface tension was taken as 0.485 N/m [12]. The same pressures were also used in the measurement with the standard MIP testing sequence. The measurement was carried out with a pressurization from 0.004 MPa to 200 MPa and then a depressurization from 200 MPa to 0.15 MPa.

4.3. BSE image analysis

Pore size distribution obtained from stereology analysis based on BSE image is used to compare with PDC-MIP results. The procedure for sample preparation and image acquisition is described as follows. The freeze-dried samples were vacuum impregnated with a low viscosity epoxy. The samples were then ground on sand papers and polished with diamond paste. For each sample, fifteen BSE images were captured at different locations in the magnification of 500×. The image segmentation was used to convert BSE images into binary images and to segregate pore structure. Pore size distribution was calculated on the binary images with a commercial program. The procedure of BSE image analysis was discussed in detail in [11].

Table 1
Advancing and receding contact angles of a 0.4-w/c-ratio Portland cement paste at the ages of 1, 3, 7 and 28 days [10].

Contact angle	Age (day)			
	1	3	7	28
Advancing	125.4°	131.1°	133.6°	138.0°
Receding	118.8°	122.6°	124.5°	128.0°

5. Results of PDC-testing sequence

In this section, the experimental results of PDC-MIP testing sequence are reported and compared with those of the standard MIP testing sequence.

5.1. Experimental results of the PDC-MIP testing sequence

5.1.1. Overall results

Fig. 4 shows the raw data of a PDC-MIP measurement. In order to show the mercury intrusion and extrusion processes within one pressurization–depressurization cycle in details, Fig. 4 (right) plots the mercury intrusion and extrusion volumes at the applied pressure of 2-4 MPa. In general, the higher the applied pressure is, the more mercury intrudes into the samples. Within one pressurization–depressurization cycle, the intrusion volume at the pressure P_n^{in} is always larger than the extrusion volume at the pressure P_n^{ex}. And, the cumulative intrusion volume at the pressure P_n^{ex} is always larger than the cumulative intrusion volume P_{n-1}^{in} in the last pressurization–depressurization cycle. The reason is that as the applied pressure increases to P_n^{in}, mercury intrudes into throat pores and ink-bottle pores behind these throat pores. Then the applied pressure decreases to P_n^{ex}. Only the mercury in the throat pores comes out, and the rest newly intruded mercury remains in the ink-bottle pores. When the applied pressure increases again to P_{n+1}^{in}, the mercury first fills in the emptied throat pores with the diameter of D_n and then fills to the pore throats with the smaller diameter of D_{n+1} and the ink-bottle pores behind these throat pores.

5.1.2. Volumes of throat pores and ink-bottle pores

By repeating the pressurization–depressurization cycles, the volumes of throat pores and ink-bottle pores can be determined as shown in Figs. 5 and 6. As the curing age increases, the throat pore volume decreases. Generally, the ink-bottle pore volume also follows this trend except that at day 1. The volume fractions of throat pores and ink-bottle pores are plotted in Fig. 7. It is found that as the curing age increases in the first 28 days, the fraction of throat pores decreases from 29% to 11%, and the fraction of ink-bottle pores increases from 71% to 89%. As shown in Figs. 5 (right) and 6 (right), the peaks in the differential throat pore volume and ink-bottle pore volume curves shift to smaller pore diameter from 1 to 28 days. This indicates that not only the throat pore size becomes smaller, but also the ink-bottles are accessed through throat pores with a decreasing pore diameter. As the cement continuously hydrates and the hydration products grow in the pore system, throat pores and ink-bottle pores are gradually filled with the hydration products.

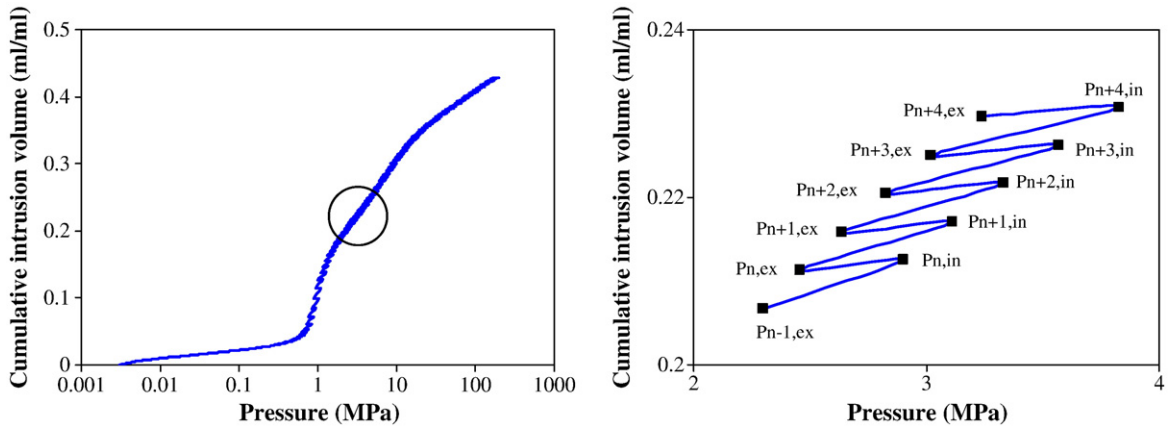

Fig. 4. Cumulative mercury intrusion vs. applied pressure curve of a 1-day-old 0.4-w/c-ratio Portland cement paste measured by PDC-MIP.

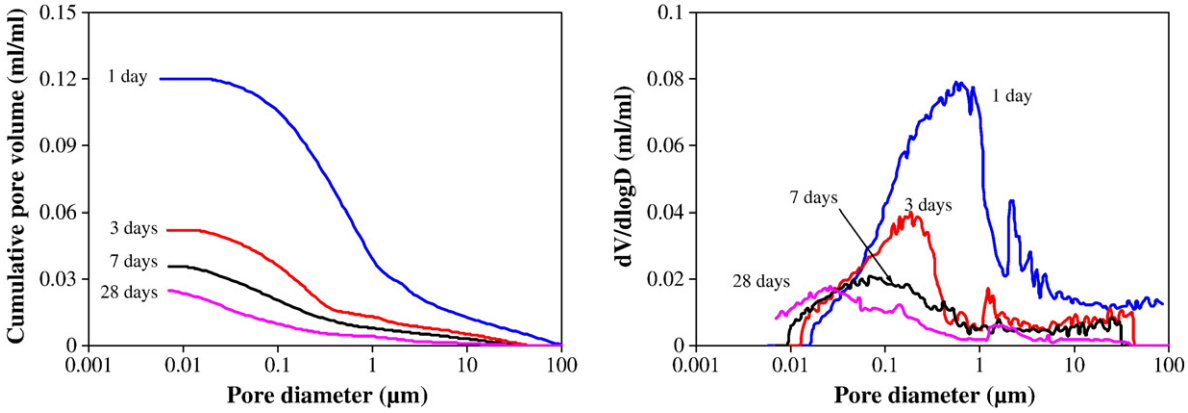

Fig. 5. Throat pore volume measured following the PDC-MIP testing sequence.

5.2. Comparison of the PDC-MIP and standard MIP testing sequences

5.2.1. Intrusion curve

Fig. 8 shows a comparison of the mercury intrusion curves of the PDC-MIP and standard MIP testing sequences. In this figure, for the PDC-MIP testing sequence, only the mercury intrusion volumes in every pressurization–depressurization cycles are plotted against the pore diameter. Regardless of the curing age, the results of these two testing sequences show a small difference in total porosities, which is lower than 1%. The total porosity decreases from 41% to 22% from 1 day to 28 days. Both the cumulative pore volume curves and the differential pore size distribution curves of the two testing sequences are very close to each other. This means that the different testing sequences do not have any influence on the mercury intrusion process.

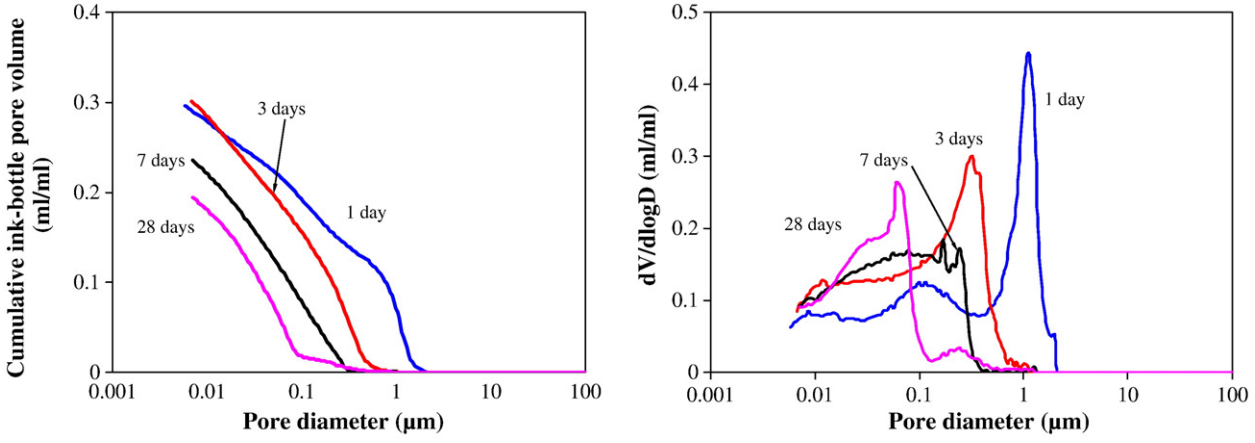

Fig. 6. Ink-bottle pore volume measured following the PDC-MIP testing sequence.

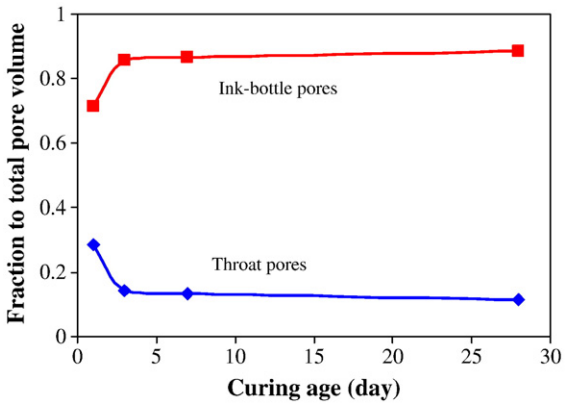

Fig. 7. Volume fractions of throat pores and ink-bottle pores.

5.2.2. Extrusion curve

The mercury extrusion curve measured following the PDC-MIP testing sequence is compared with that measured following the standard MIP testing sequence as shown in Fig. 9. The PDC-MIP measurement gives much lower mercury extrusion volumes than the standard MIP measurement. When pressure is decreased, the throat pores first get empty and the ink-bottle pores behind the throat pores remain filled because the decreased pressure is not great enough to force mercury to go through the throat pores. Until pressure continues to decrease to a certain value at which mercury overcomes the restriction of throat pores, mercury comes out of the ink-bottle pores [13]. Some ink-bottle pores may not get empty at all even at the minimum pressure, if the ink-bottle pores and the connected throat pores have inappropriate sizes. In every pressurization–depressurization cycle, the pressure decrease is tailored to only empty the throat pores rather than the ink-bottle pores. In contrast, for the standard MIP pressure is continuously decreased to the minimum pressure, mercury in some ink-bottle pores can thus go through throat pores and comes out of the sample. Therefore, in the depressurization process of the standard MIP the measured extrusion volume is the sum of the volumes of all throat pores and some of the ink-bottle pores.

6. Pore size distribution calculated by the PDC-MIP data analysis method

This section reports the pore size distribution calculated by the PDC-MIP data analysis method. PDC-MIP is further validated by nitrogen sorption, BSE image analysis, WMIP and numerical simulation with HYMOSTRUC3D.

6.1. Pore size distribution calculated by the PDC-MIP data analysis method

Fig. 10 shows the pore size distribution calculated using Eqs. (4)–(8a,8b). Most pores distribute at the diameter ranging from 0.1 to 10 μm. As expected, pore size becomes smaller, as the curing age increases. From 1 day to 28 days, the critical pore size measured by PDC-MIP decreases from 3.2 μm–1.2 μm to 0.42 μm–0.14 μm. It is also observed that the volume of large pores decreases, and the volume of small pores increases. This observation agrees with the well documented phenomena, that the formation and growth of hydration products in the pore space result in the decrease of the volume of large pore and the pore diameter.

6.2. Comparison of the pore size distribution measured by PDC-MIP with other experimental techniques and numerical tool

6.2.1. Compared with nitrogen sorption and 2nd mercury intrusion

Nitrogen sorption is another popular technique used to investigate the pore structure. However, pore radius ranges detected by nitrogen sorption (0.3–300 nm) are narrower than that by MIP (2 nm–100 μm). Consequently, the total porosity determined by nitrogen sorption is lower than that determined by MIP [14]. Kaufmann et al. [15] recently found that the pore size distribution obtained by nitrogen sorption agreed well with that obtained by 2nd mercury intrusion, when mercury intrusion–extrusion cycle was repeated twice (as shown in Fig. 11). The "accessibility effect" was considered to be reduced in the 2nd mercury intrusion, since the ink-bottle pores were already filled in the first intrusion–extrusion cycle.

Since the pore size distribution of 0.4-w/c-ratio Portland cement pastes measured by nitrogen sorption is not available, the results of PDC-MIP and standard MIP are only compared with that of 2nd mercury intrusion, which comes from [11]. As shown in Fig. 12, it is obvious that the pore size distribution obtained by 2nd mercury intrusion agrees better with that of PDC-MIP than standard MIP. Considering the good agreement of the results of nitrogen sorption and 2nd mercury intrusion, the pore size distribution obtained by PDC-MIP might agree well with that obtained by nitrogen sorption.

6.2.2. Compared with BSE image analysis

Scanning electron microscopy (SEM), particularly using BSE technique, has been applied extensively to study the pore structure of cement-based materials [11,16,17]. This technique can provide two-dimensional information of porosity by capturing the images

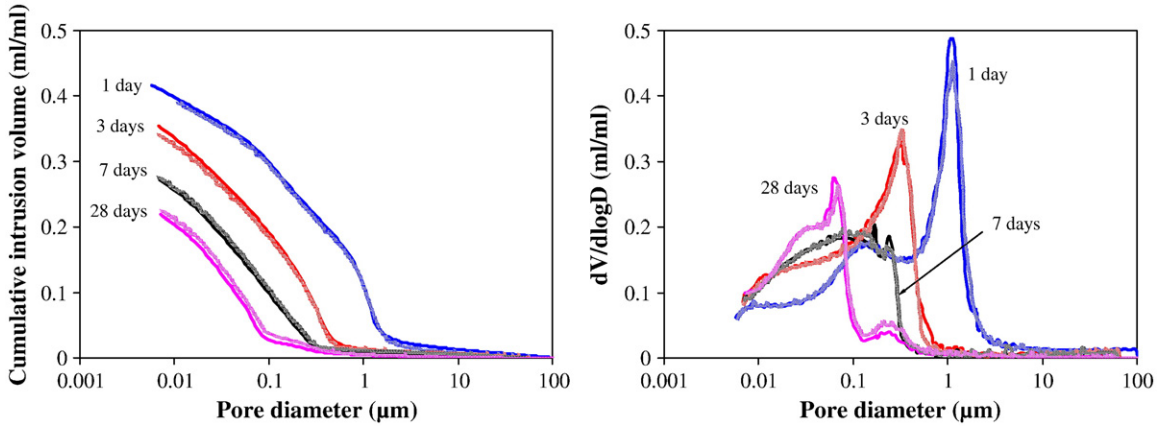

Fig. 8. Mercury intrusion curves measured following the PDC-MIP and standard MIP testing sequences.

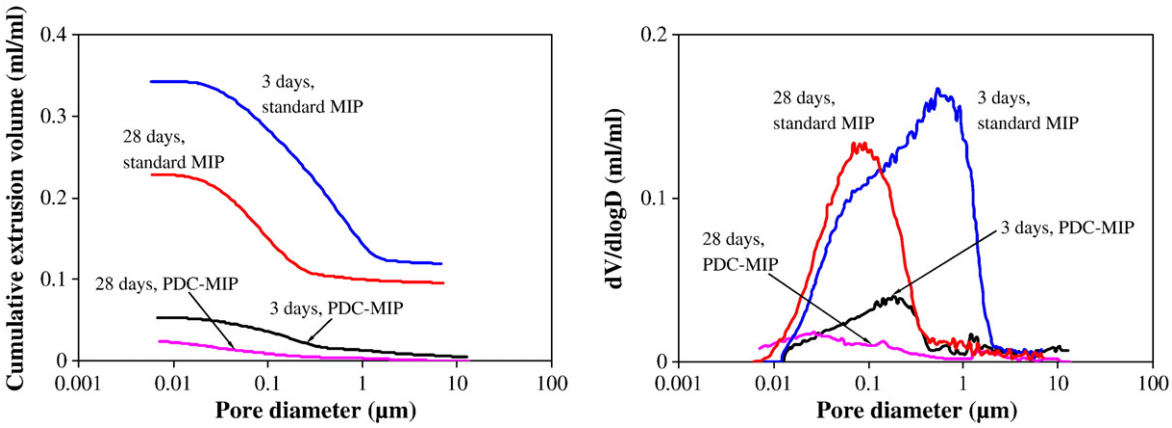

Fig. 9. Mercury extrusion curves measured following the PDC-MIP and standard MIP testing sequences.

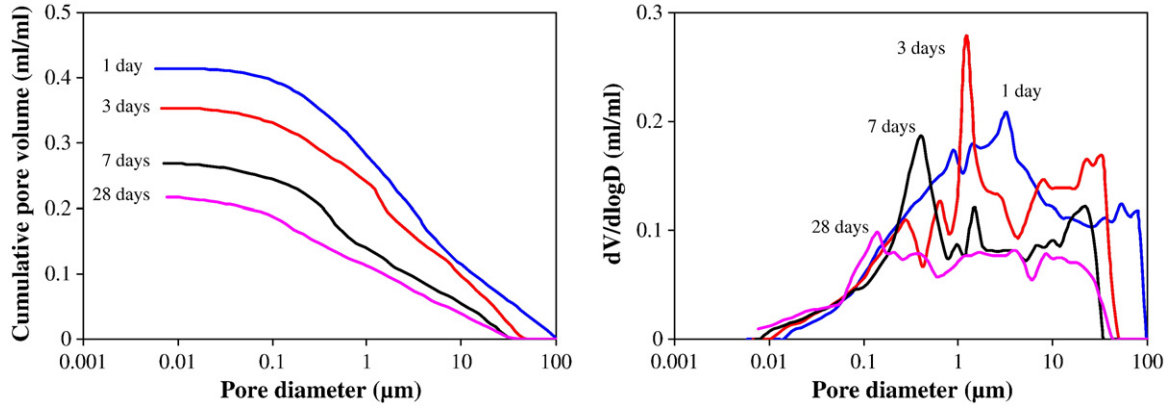

Fig. 10. Pore size distributions of 0.4-w/c-ratio Portland cement pastes at the ages of 1, 3, 7 and 28 days measured by PDC-MIP.

directly from the pore structure. According to the stereology theory [18,19], the three-dimensional information of pore structure can be derived from the two-dimensional BSE images. Fig. 13 illustrates a comparison of the pore size distributions measured by PDC-MIP, standard MIP and BSE image analysis. The total porosities measured by PDC-MIP and standard MIP are higher than that measured by BSE image analysis. PDC-MIP and standard MIP give total porosities from 41% to 22% at the ages of 1–28 days, while BSE image analysis gives total porosities from 33% to 16%. Due to the resolution limit of BSE images, the pores with a diameter smaller than 0.25 μm are not detectable. Therefore, the lower porosity measured by BSE image analysis can be partially attributed to the incomplete measurement. Regardless of the curing age, the result of PDC-MIP shows a critical pore diameter larger than that of standard MIP and smaller than that of BSE image analysis. For example, for the 3-day sample, the standard MIP measurement allocates most pores below 1 μm with the critical pore size of 0.32 μm, the PDC-MIP measurement allocates most pores between 0.1 μm and 50 μm with the critical pore size of 1.2 μm, and BSE image analysis allocates most pores bigger than 0.25 μm with the critical pore size of 4.5 μm.

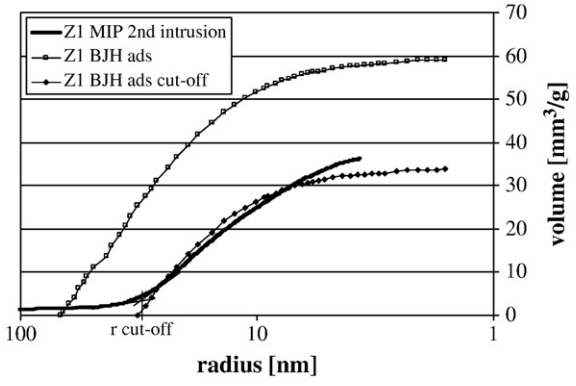

Fig. 11. Pore size distributions of a 28-day-old 0.3-w/c-ratio Portland cement paste obtained by 2nd mercury intrusion and calculated using BJH theory from nitrogen sorption data [15].

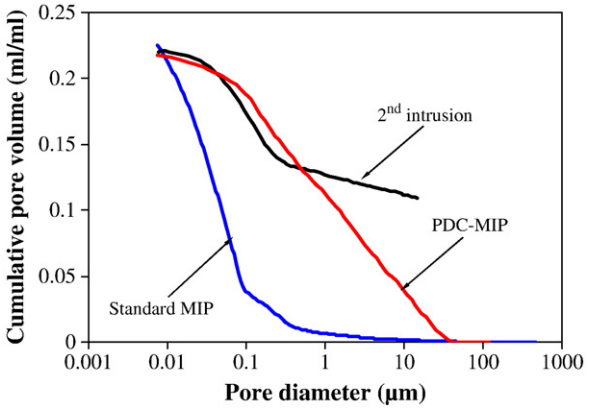

Fig. 12. Pore size distributions of a 28-day-old 0.4-w/c-ratio Portland cement paste measured by PDC-MIP, standard MIP and 2nd mercury intrusion (after Ye [11]).

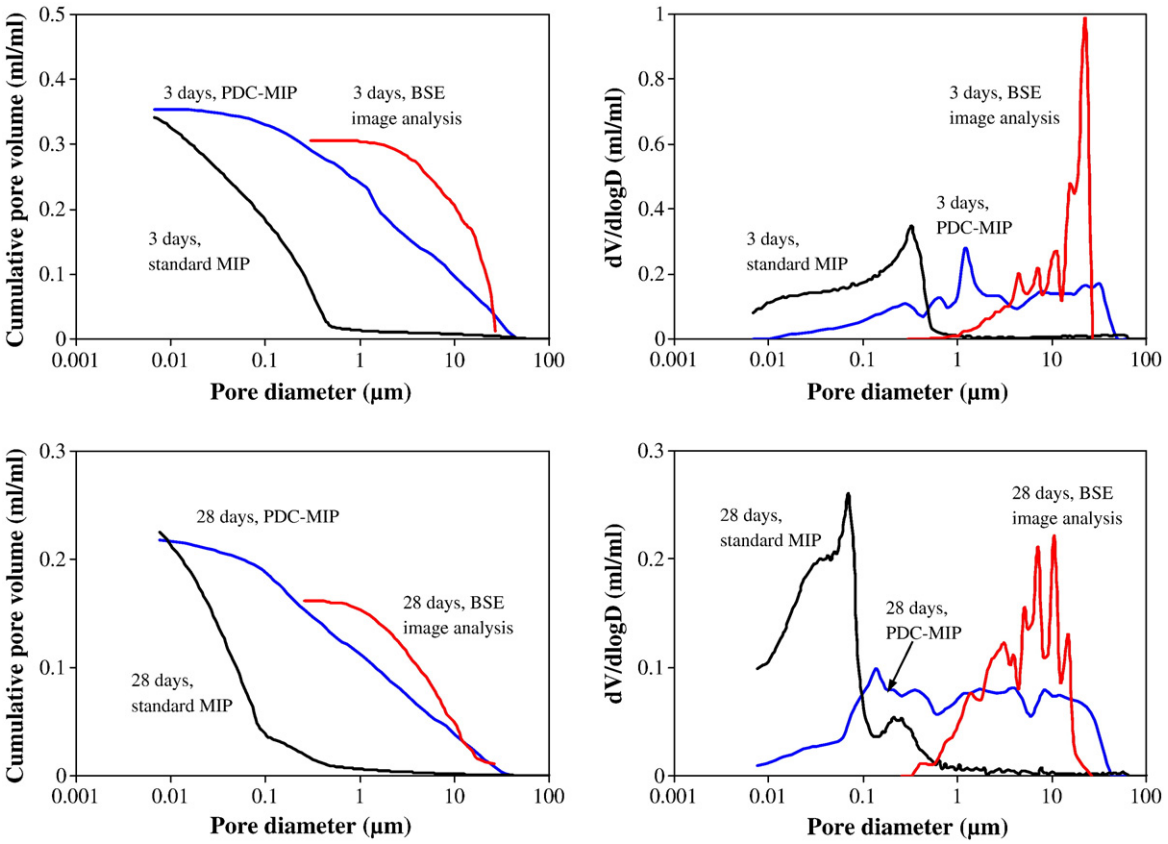

Fig. 13. Pore size distributions of 0.4-w/c-ratio Portland cement pastes at the ages of 3 and 28 days obtained by PDC-MIP, standard MIP and BSE image analysis.

6.2.3. Compared with WMIP

The combination of WMIP and BSE image analysis, a relatively new technique, has shown a potential to characterize the pore structure. It has been confirmed that this technique can provide a reasonable estimation of pore size distribution [20,21]. This technique was used by Willis et al. [20] to study the pore size distribution of mortar samples. Under a pressure of 34 MPa, molten Wood's metal was forced to intrude into the samples. After cooling, the intruded Wood's metal solidified. Images were captured on the sections of the Wood's-metal-intruded samples by SEM. On these images, the Wood's-metal-intruded pore structure appeared bright, and other phases appeared relatively dark. The pore structure was segmented from other phases according to their grey levels. The pore size distribution was determined on these segmented images. In [20], Willis et al. reported the fraction of pore volume to the volume of mortar samples. For comparison, this value is converted to the fraction of pore volume to the volume of cement paste based on the cement paste content in the mortar samples. Fig. 14 illustrates a comparison of the results of PDC-MIP, standard MIP and WMIP. The pore size distribution of PDC-MIP shows a much better agreement with that of WMIP compared with standard MIP. The pores measured by the former two methods are mostly in the sizes of 0.1–10 μm, while the pores measured by standard MIP are mostly smaller that 0.1 μm. This agrees with the conclusion of Willis et al. [20], which states that "the size distributions obtained from MIP are shifted more towards smaller pores than those obtained from WMIP and image analysis".

6.2.4. Compared with numerical simulation by HYMOSTRUC3D

The cement hydration model HYMOSTRUC3D [11,22,23] was developed to simulate the reaction process and microstructure development of cement-based materials with different material compositions (such as, w/c-ratio, chemical composition of cement, blended materials and particle fineness) at different scales (micro and macro). This model has been confirmed to be a good tool for understanding the development of the microstructure, particularly the pore structure of cement-based materials [11]. The results of numerical simulation by HYMOSTRUC3D are used to validate PDC-MIP. In the simulated microstructure, the pore space is the free space between the expanding cement grains. The pore size distribution is determined by calculating the sub-volumes of the pore space that are accessible to testing spheres of different diameters [11]. In this study, the pore size distribution of a 28-day-old 0.4-w/c-ratio Portland cement paste is calculated by the HYMOSTRUC3D model. Fig. 15 shows a comparison of

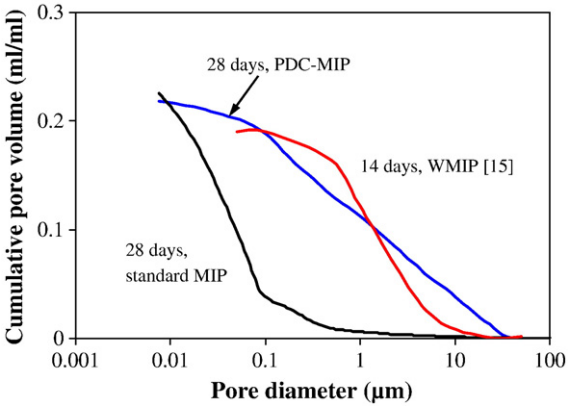

Fig. 14. Pore size distributions measured by PDC-MIP, standard MIP and WMIP (after Willis et al. [20]).

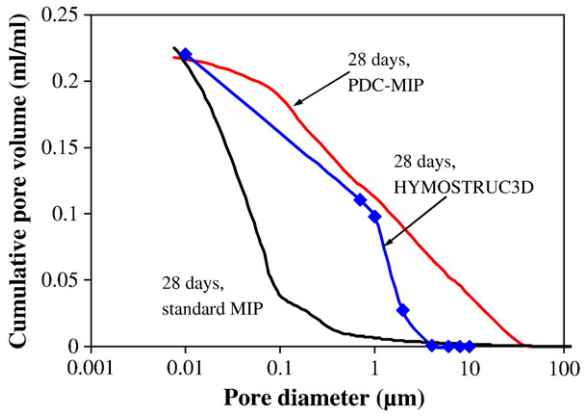

Fig. 15. Pore size distributions of a 28-day-old 0.4-w/c-ratio Portland cement pastes obtained by PDC-MIP, standard MIP and the numerical simulation by HYMOSTRUC3D.

the pore size distributions obtained by PDC-MIP, standard MIP and the numerical simulation by the HYMOSTRUC3D model. The pore sizes calculated by the numerical simulation are a bit smaller than that measured by PDC-MIP and much larger than that measured by standard MIP. The pore size distributions obtained from the numerical simulation and PDC-MIP agree well with each other, compared with standard MIP.

7. Discussion

Compared with standard MIP, PDC-MIP has a better agreement on pore size distribution with nitrogen sorption, BSE image analysis, WMIP and numerical simulation. It is found that the pore sizes measured by PDC-MIP are larger than those measured by standard MIP. The smaller pore size measured by standard MIP can be attributed to the "accessibility effect", which results in overestimating the volume of smaller pores and underestimating the volume of larger pores. The above discussion confirms that PDC-MIP can eliminate the impact of the "accessibility effect" and improve the MIP technique on measuring pore size distribution.

8. Conclusions

The PDC-MIP method is developed aiming to eliminate the "accessibility effect" on the estimation of the pore size distribution in cement-based materials. PDC-MIP is used to investigate the pore structure of Portland cement pastes. The experimental results of PDC-MIP are compared with those of standard MIP, nitrogen sorption, BSE image analysis, WMIP and the numerical simulation by the HYMOSTRUC3D model. Based on the results and discussion presented in this paper, the following conclusions can be drawn:

1. PDC-MIP can be used to determine the volumes of throat pores and ink-bottle pores at every pore sizes. In a 0.4-w/c-ratio Portland cement paste as the curing age increases from 1 day to 28 days, the volume fraction of throat pores decreases from 29% to 11%, and the volume fraction of ink-bottle pores increases from 71% to 89%.
2. Compared with standard MIP, the pore size distribution measured by PDC-MIP has a better agreement with that obtained from nitrogen sorption, BSE image analysis, WMIP and the numerical simulation by the HYMOSTRUC3D model.
3. PDC-MIP can eliminate the impact of the "accessibility effect" and improve the MIP technique on measuring the pore size distribution in porous materials, especially cement-based materials.

References

[1] S. Mindess, J.F. Young, Concrete, Prentice-Hall, Englewood Cliffs, NJ, 1981.
[2] A.M. Neville, Properties of Concrete, 4th ed.Wiley, New York, 1995.
[3] D.N. Winslow, S. Diamond, A mercury porosimetry study of evolution of porosity in Portland cement, J. Mater. 5 (3) (1970) 564–585.
[4] E.W. Washburn, Note on a method of determining the distribution of pore sizes in a porous material, Porc. Natl. Acad. Sci. USA 7 (1921) 115–116.
[5] L. Cui, J.H. Cahyadi, Permeability and pore structure of OPC pastes, Cem. Concr. Res. 31 (2) (2001) 277–282.
[6] S. Diamond, Mercury porosimetry — an inappropriate method for the measurement of pore size distributions in cement-based materials, Cem. Concr. Res. 30 (10) (2000) 1517–1525.
[7] F. Moro, H. Bohni, Ink-bottle effect in mercury intrusion porosimetry of cement-based materials, J. Colloid Interface Sci. 246 (1) (2002) 135–149.
[8] Z. Liu, D. Winslow, Sub-distributions of pore size: a new approach to correlate pore structure with permeability, Cem. Concr. Res. 25 (4) (1995) 769–778.
[9] R. Yoshida, T. Kishi, Proposal of a New Approach for Determination of Pore Continuity and Suitable Intrusion Pressure Based on Step-By-Step Mercury Intrusion Porosity Test, in: W. Sun, et al., (Eds.), Proc. 1st International Conference on Microstructure Related Durability of Cementitious Composites, Nanjing, China, 2008, pp. 1455–1464.
[10] J. Zhou, G. Ye, E. Schlangen, K. van Breugel, Advancing and receding contact angles between mercury and cement-based materials, in draft.
[11] G. Ye, Experimental Study and Numerical Simulation of the Development of the Microstructure and Permeability of Cementitious Materials, Ph.D. Thesis, Delft University Press, Delft, 2003. Available on http://Microlab.citg.tudelft.nl.
[12] D.R. Lide, CRC Handbook of Chemistry and Physics, 84th Edition, CRC Press, Boca Roton, 2003.
[13] P.A. Webb, An Introduction to the Physical Characterization of Materials by Mercury Intrusion Porosimetry with Emphasis on Reduction and Presentation of Experimental Data, Micromeritics Instrument Corp, Georgia, 2001 Available on http://www.particletesting.com/docs/intro_mip.pdf.
[14] K.K. Aligizaki, Pore Structure of Cement-Based Materials, Taylor & Francis, London, 2006.
[15] J. Kaufmann, R. Loser, A. Leemann, Analysis of cement-bonded materials by multi-cycle mercury intrusion and nitrogen sorption, J. Colloid Interface Sci. 336 (2009) 730–737.
[16] D.A. Lange, H.M. Jennings, S.P. Shah, Image analysis techniques for characterization of pore structure of cement-based materials, Cem. Concr. Res. 24 (5) (1994) 841–853.
[17] S. Diamond, M.E. Leeman, Pore Size Distributions in Hardened Cement Paste by Sem Image Analysis, in: S. Diamond, et al., (Eds.), Proc. Materials Research Society Symposia 370, Microstructure of Cement-Based Systems/Bonding and Interfaces in Cement-Based Materials, 1995, pp. 217–226.
[18] E.E. Underwood, Quantitative Stereology, Addison-Wesley, Massachusetts, 1970.
[19] S. Diamond, M.E. Leeman, Pore size distribution in hardened cement paste by SEM image analysis, Proc. Materials Research Society Symposia 370 (1995) 217–226.
[20] K.L. Willis, A.B. Abell, D.A. Lange, Image-based characterization of cement pore structure using Wood's metal intrusion, Cem. Concr. Res. 28 (12) (1998) 1695–1706.
[21] A.B. Abell, K.L. Willis, D.A. Lange, Mercury intrusion porosimetry and image analysis of cement-based materials, J. Colloid Interface Sci. 211 (1) (1999) 39–44.
[22] K. van Breugel, Simulation of Hydration and Formation of Structure in Hardening Cement-Based Materials, PhD theses, Delft University of Technology, Delft, 1991. Available on http://Microlab.citg.tudelft.nl.
[23] E. Koenders, Simulation of Volume Changes in Hardening Cement-Based Materials, PhD thesis, Delft University of Technology, Delft, 1997. Available on http://Microlab.citg.tudelft.nl.